Nanoscale Reduction of Graphene Fluoride *via* Thermochemical Nanolithography

Woo-Kyung Lee,[†,*] Michael Haydell,[‡] Jeremy T. Robinson,[†] Arnaldo R. Laracuente,[†] Elena Cimpoiasu,[‡] William P. King,[§] and Paul E. Sheehan[†]

[†]U.S. Naval Research Laboratory, Washington, D.C. 20375, United States, [‡]Department of Physics, U.S. Naval Academy, Annapolis, Maryland 21402, United States, and [§]Department of Mechanical Science and Engineering, University of Illinois, Urbana—Champaign, Illinois 61801, United States

ABSTRACT Graphene nanoribbons (GNRs) would be the ideal building blocks for all carbon electronics; however, many challenges remain in developing an appropriate nanolithography that generates high-quality ribbons in registry with other devices. Here we report direct and local fabrication of GNRs by thermochemical nanolithography, which uses a heated AFM probe to locally convert highly insulating graphene fluoride to conductive graphene. Chemically isolated GNRs as narrow as 40 nm show p-doping behavior and sheet resistances as low as 22.9 KΩ/□ in air, only approximately 10× higher than that of pristine graphene. The impact of probe temperature and speed are examined as well as the variable-temperature transport properties of the GNR.

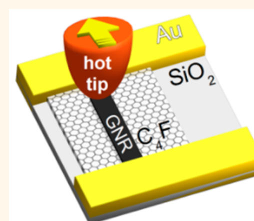

KEYWORDS: graphene nanoribbons · graphene fluoride · thermochemical nanolithography · atomic force microscopy

Graphene nanoribbons (GNRs) have been extensively studied as potential building blocks for all-carbon nanoelectronics. This interest stems both from the ability to open a band gap in GNRs due to size confinement[1] and from the potential for greater control over size and defined interconnectivity between GNR devices. Multiple lithographies for patterning GNRs have been introduced such as electron beam lithography (EBL),[1] shattering exfoliated graphite by ultrasonication,[2] unzipping carbon nanotubes,[3] and nanowire masks.[4,5] These methods achieved significant progress in generating narrow GNRs; however, each has its own drawbacks, which can include low yield, contamination, defects, and rough edges.

A generic challenge with these techniques is that, excepting EBL, they do not provide a robust means to place GNRs with precision. EBL's high accuracy comes at the cost of implementing etching and lift-off procedures that generally damage the GNR edges and leave extrinsic residues on their surface. A second challenge is that most lithographic approaches geometrically isolate the GNRs by cutting it out of a larger graphene sheet rather than chemically isolating the nanoribbons within a larger film of insulating chemically modified graphene (CMG). The benefits of chemical isolation include stabilization of the nanoribbons edges to prevent unintentional doping as well as the potential to reset chemically the graphene/CMG sheet for rewriteable electronics.[6] The search for a nanolithography with precise placement capabilities has inspired the use of scanning probe techniques that first image then modify a graphene film to form GNRs. Recently, Hou *et al.*[7] reported a platinum AFM tip could locally reduce GO film at 115 °C under a hydrogen environment. This approach uses the local catalytic activity of a Pt tip in the presence of hydrogen to accelerate the reduction of GO. In 2010, we introduced thermochemical nanolithography (TCNL), where a heated probe directly reduces insulating graphene oxide (GO) to graphene ribbons with ~12 nm resolution.[8] This technique uses robust AFM probes with excellent wear resistance,[9] large CVD graphene, and large-scale chemical functionalization, and so is a direct fabrication method amenable to large-scale fabrication.

While conceptually straightforward, our initial TCNL approach to GNR lithography faced a significant difficulty in that it used graphene oxide, which does not reduce completely to graphene, but rather forms a compound commonly referred to as

* Address correspondence to woo.lee@nrl.navy.mil.

Received for review April 30, 2013 and accepted June 12, 2013.

Published online June 12, 2013
10.1021/nn4021746

© 2013 American Chemical Society

reduced graphene oxide (rGO), where residual oxygen (even after thermal annealing at 1500 K) is still incorporated into the lattice.[10] Given our recent success in nearly completely restoring graphene fluoride to graphene with hydrazine,[6] we sought to improve the performance of the TCNL approach using this newer material. Graphene fluoride (GF) can be readily obtained by exposing graphene to XeF_2 gas in a commercially available system (Xactic etcher).[11] The GF is fairly stable, but also amenable to subsequent reactions to modulate the surface chemistry and potentially its doping.[12] Importantly, although there are other chemically modified graphenes such as graphane[13] and aminated graphene,[14] only oxygenated and fluorinated graphene have shown sufficient suppression of conductivity (resistivity increase > $\sim 10^9$ Ω) to generate electronic devices defined *via* TCNL.[7,8] Using GF, Withers *et al.*[15] recently demonstrated direct reduction *via* electron beam irradiation. The sheet resistance of the reduced area could be as low as 100 kΩ/□ when irradiated with an electron dose of 1 C/cm^2. Although this reduction requires a fairly high dose, it represented significant progress in establishing GF as a facile lithographic platform.

In this paper, we demonstrate the use of TCNL to locally reduce GF. The final structures were chemically isolated GNRs surrounded by GF. The sheet resistivity of GNRs with widths from 40 to 200 nm could be lowered to ~22.9 kΩ/□, only ~10× higher than that of the starting CVD graphene. To the best of our knowledge, this constitutes the most effective direct reduction of a chemically modified graphene reported to date. The ribbons were also reproducibly p-doped due to the contiguous GF as shown in prior work.[6] Compared with previous TCNL of GO, TCNL could reduce GF more effectively presumably due to the greater chemical homogeneity and the inability of the fluorine to incorporate into the backbone of the graphene lattice. Finally, we show that the more simple chemistry enables efficient reduction of the graphene over a narrower thermal processing window and at lower temperature than GO.

RESULTS AND DISCUSSION

We fabricated micrometer scale graphene field effect transistors to serve as base devices by transferring CVD-grown monolayer graphene onto a SiO_2/Si substrate and performing conventional lift-off lithography. The transport properties of these base devices were measured, and then the graphene was made insulating *via* fluorination such that the base device registered as an open circuit (resistance >1 TΩ). TCNL then locally restored the graphene and, thus, conductivity along thin ribbons. Figure 1 shows a graphene nanoribbon created with a ~600 °C probe moving at 20 nm/s under N_2. All TCNL was performed under inert environments to minimize possible reactions with water or oxygen

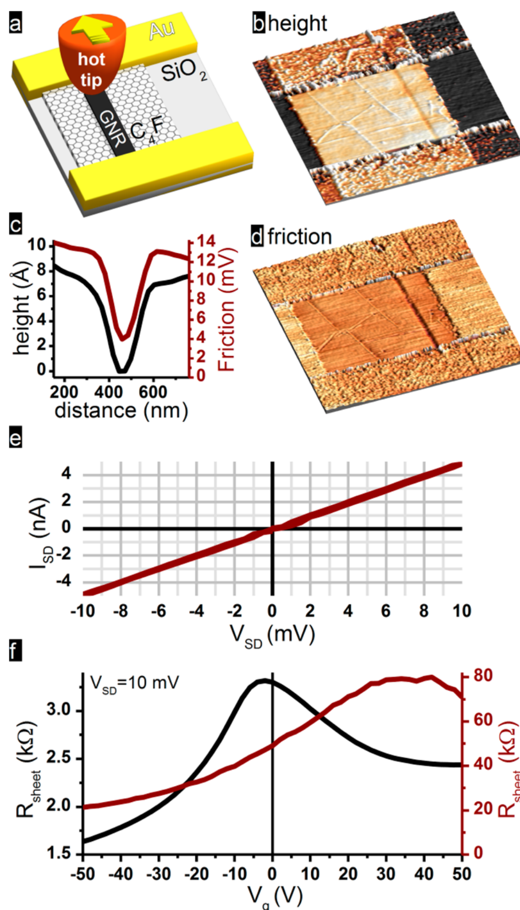

Figure 1. Thermochemical nanolithography (TCNL) of graphene fluoride (GF). (a) Schematic diagram illustrating TCNL on a prefabricated single-layered graphene device. (b) AFM height image of a reduced ribbon. (c) Cross-sectional profile of height and friction images. (d) AFM friction image of a reduced ribbon. (e) *IV* characteristics of the reduced device by TCNL shown in (b) and (d). (f) R_{sheet} *vs* gate voltage characteristics of the reduced device; base device (prefluorination) in black and reduced device from GF in red. Note that slight hysteresis produces different values at zero gate bias between (f) and (e).

found in the ambient. The reduced GF nanoribbon was ~120 nm wide and 0.65 nm deep against the background GF, as shown in Figure 1c. There are several observations to support that the heated probe removed fluorine. First, the lower height is consistent with the loss of pendant fluorine, as well as a flattening of the lattice as it shifts from sp^3- to sp^2-hybridization. This value compares favorably to the 0.7 nm height reduction when fluorine was removed by electron beam exposure.[15] Second, the friction image (Figure 1d) shows lower friction (dark) than background GF (bright), which is consistent with results from bulk fluorinated and pristine graphene.[16] This reduction in friction was observed previously with TCNL of GO[8] and is consistent with recent reports showing that GF has a higher friction coefficient than pristine graphene.[16] Finally, a more direct indication of a chemical change to graphene is the decreased resistivity: the resistance of the reduced line in Figure 1b was approximately 2.08 MΩ *versus* a starting

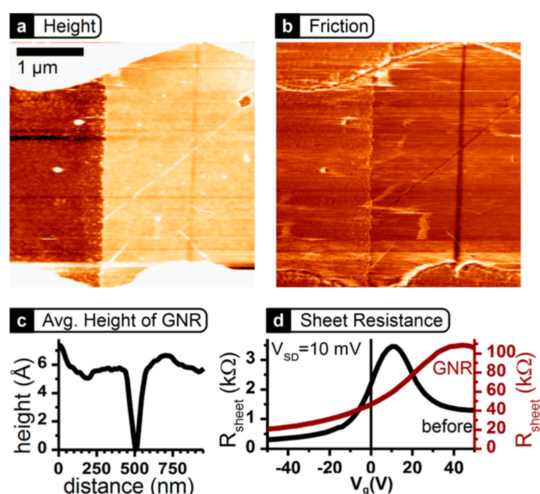

Figure 2. TCNL of GF under 10% hydrogen in argon environment. (a) AFM height image of a reduced ribbon with 60 nm width, (b) corresponding friction image of (a), (c) cross-sectional profile of (a), and (d) R_{sheet} *vs* gate voltage of the device shown in (a) and (b).

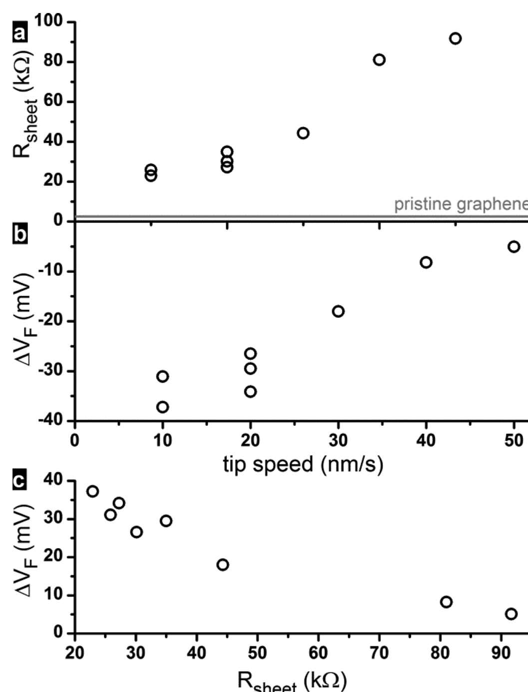

Figure 3. TCNL controls: (a) dependence of R_{sheet} upon tip writing speeds from 10 to 50 nm/s under 10% hydrogen in Ar, (b) frictional signal change (ΔV_F) in AFM friction image as a function of tip writing speeds, and (c) the relationship between the frictional signal change (ΔV_F) and R_{sheet}.

resistance of >1 TΩ. In Figure 1f, the sheet resistance (R_{sheet}) *versus* gate voltage characteristics reveal a 62.4 kΩ/□ at zero gate voltage (V_g). Given the starting R_{sheet} of ~2−3 kΩ/□ at 0 V_g, this indicates that the GNR may be incompletely reduced or that other scattering defects are introduced during reduction. In addition to the slight increase in resistance, the Dirac point shifted to more positive V_g, a result of p-doping by the neighboring fluorine.[6] The details of reduced GF were examined with Raman spectroscopy after writing a large square (see Supporting Information, S1).

To improve the reduction process, we examined the effect of the ambient atmosphere during TCNL. For graphene oxide, it is known that treatment in an H_2-containing gas mixture enhances reduction.[6,11,17] Figure 2 shows the writing of a graphene ribbon *via* TCNL using the same experimental conditions as shown in Figure 1 except under 10% H_2/Ar gas mixture. Again, lowered heights and lateral forces indicated successful fluorine reduction to form a 60 nm wide line. Critically, the R_{sheet} at 0 V_g was ~40 kΩ, approximately half that of the GNR produced under N_2, which supports the notion that better reduction occurs under 10% H_2/Ar compared to N_2. Comparing numerous devices reduced using either N_2 or H_2/Ar, we find the lowest R_{sheet} for N_2 is ~47 kΩ/□, while those reduced under 10% H_2/Ar achieved resistances of ~22.9 kΩ/□ (Figure 3). Prior reports[11,17] have noted that the reduction of GF could be achieved efficiently with the presence of hydrogen as compared with their Raman spectra. Given the improved performance under 10% H_2/Ar, all subsequent experiments were carried out under that reducing ambient.

To further optimize GNR electrical properties, we examined the relationship between writing speed and probe temperature on reduction (Figure 3). To study the impact of speed, multiple GNR devices were made while the heated probe was scanned from 10 to 50 nm/s at 600 °C. Note that this temperature is the cantilever temperature; the temperature at the probe/surface interface is considerably less but may be estimated.[8] For GF processed under H_2/Ar, the R_{sheet} increased roughly linearly with tip speed (Figure 3a) within the above-mentioned range. However, the direct correlation between R_{sheet} and lattice defect density, and thus the degree of reduction, is currently unknown. We note that the minimum R_{sheet} achieved in this work, 22.9 kΩ/□, improves on the prior work on GO, which had R_{sheet} = 65 kΩ/□ for *multilayered* rGO, which would intrinsically show a lower sheet resistance due to its greater thickness. Similarly, a reduced GNR (80 nm) written from GO at the speed of 1 nm/s *via* catalytic scanning probe lithography could achieve a much higher R_{sheet} of only >2.5 MΩ/□. Even though thermal reduction appears to offer a more complete local reduction, the 10-fold increase in resistivity over the base devices (R_{sheet} = 2−3 kΩ) suggests that either some fluorine remains after the process or defects are introduced during fluorine removal. Finally, Figure 3b clearly shows that reduction is inversely proportional to tip speed, as measured by friction differences between the GNR and the contiguous graphene fluoride (ΔV_F).

The effect of tip temperature (T_{tip}) on fluorine removal was examined by writing seven 250 × 500 nm^2 rectangular areas on a large GF sheet using T_{tip} = 200 to

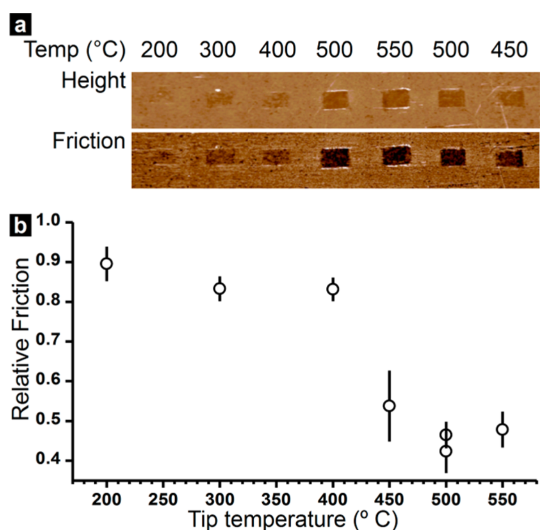

Figure 4. TCNL controlled by probe temperature. (a) Sequentially written 250 × 500 nm rectangles with the probe held at different temperatures. The tip writing speed was 250 nm/s. The reduction was accelerated above the threshold temperature of approximately 400 °C. (b) Plot of the friction of the reduced GF rectangles relative to the adjacent GF. The friction data were obtained by subtracting the data for trace and retrace scan directions.

550 °C (Figure 4). As shown in the friction images, minimal friction changes are observed at temperatures between 200 and 400 °C; however, there was a relatively sharp onset of reduction at T_{tip} = 400−500 °C, which tapers off after 500 °C. In comparison, GO reduction initiates at tip temperatures near 150 °C, and the reduction tapers off only at ∼750 °C.[8] The narrower thermal processing window was expected since GF has far fewer types of functional groups (mostly basal plane C−F with some C−F_2 at defects) to be removed, in contrast to GO, where there is a wide range of oxygen-rich functional groups (carbonyl, epoxides, hydroxyls, carboxyls, *etc.*) as well as water, all of which would be expected to desorb at different temperatures.[10] These results show that the kinetics of TCNL reduction may be controlled but at lower tip temperatures than for graphene oxide.

Finally, we characterized the electrical properties of a GNR device both in air at room temperature and in UHV, as a function of temperature. The carrier mobility (hole) of our GNRs measured in air was 30.3 ± 13.8 $cm^2/(V\ s)$ (8 devices). This is approximately 2 orders of magnitude lower than the base SLG devices (∼3000 $cm^2/(V\ s)$). The mobility of these GNRs are comparable with GNRs formed from GO *via* catalytic scanning probe lithography, estimated to be about 21 $cm^2/(V\ s)$.[7] Again, we assumed the lower carrier mobility mainly stems from incomplete reduction by TCNL. This could be an intrinsic limit due to the thermal removal of the fluorine; however, we cannot fully rule out the presence of PMMA polymer residues, which, if present, would add variability in the reduction process or could prevent continuous reduction. The clean

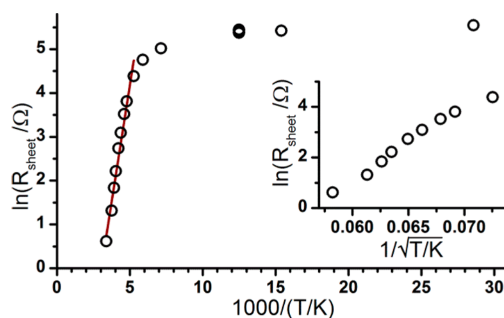

Figure 5. Temperature dependence of a reduced ribbon *via* TCNL. The plot clearly shows two distinct temperature-dependent regions, slow recovery of conductivity in the low-temperature region and thermally activated recovery of conductivity in the high-temperature region. Inset shows the sheet resistance as a function of $T^{-1/2}$ in the high-temperature region (T > 180 K).

transfer of CVD graphene is an ongoing effort in the graphene community.[18−21] For most of the work reported here we found that, if present, a thin residue layer could be removed by prescanning the area of interest with contact AFM using low load, a tedious but reproducible approach. Another limitation in the TCNL approach is the metal contact/graphene junction. We typically use ∼25 nm of Ti/Au for electrodes, which may inhibit reduction immediately at the contact junction where the tall and rough edges at the junction of GF and electrodes can cause discontinuity in reduction. Such devices showed no conductivity or high R_{sheet} due to poor reduction at the junction. While these skips would not occur when writing multiple devices on a single sheet of graphene, it still should be considered for heterogeneous integration. The use of stepped electrodes such as those used in anodic oxidation lithography[22] may help overcome this issue.

For the variable-temperature measurements, a 120 mm GNR generated *via* TCNL was loaded into a UHV nanoprobe system and cooled to 35 K while continuously measuring its resistance. The GNR was p-doped due to the contiguous graphene fluoride as previously reported. The dependence of natural log of R_{sheet} at zero bias on 1000/T is shown in Figure 5. We observe two distinct temperature dependencies: a plateau region at low temperature below approximately 80 K and a thermally activated recovery of conductivity at high temperatures. This behavior suggests that the measured conductivity is a superposition of two contributions. The low-temperature contribution, which is practically temperature independent, might arise from tunneling between high-conductivity pristine graphene islands separated by disordered low-conductivity barrier regions, as tunneling does not require thermal excitations even at zero temperature.[23,24] On the other hand, for T > 140 K, the linear dependence on 1000/T suggests a thermally activated conduction. The estimated activation energy from the Arrhenius relation is 198 ± 9 meV. Such high

activation energy indicates a partial reduction of GF and that the activation energy can be lowered with even further reduction. We also tested variable range hopping (VRH) models on the high-temperature data. The inset of Figure 5 shows that the resistance could follow a $T^{-1/2}$ dependence for $T > 180$ K as well. According to theory, such a temperature dependence corresponds to either 1D or 2D VRH in the presence of a Coulomb gap.[15,25] Attempts to fit the data to extract directly the exponent of the temperature did not converge. More detailed studies are currently under way with varied degrees of reduction of the GF.

CONCLUSIONS

We demonstrated the direct fabrication of chemically isolated GNRs *via* TCNL reduction of GF by using a heated probe. We could form GNRs as narrow as ~40 nm (see Supporting Information, S2), and the R_{sheet} was as low as ~22.9 kΩ/□ in air. We also showed the conduction mechanism of our GNRs was hopping *via* a localized state. GF is a superior candidate for TCNL reduction since a single species (C−F) dominates and the fluorine cannot incorporate into the lattice. The TCNL reduction could be enhanced with 10% H_2/Ar. Although characterization suggests that our GNRs were partially reduced graphene fluoride, we could recover its conductivity up to ~10× of its initial R_{sheet}. While this is not sufficient to restore the intrinsic properties of graphene, it would provide a route to write directly conductive traces with tunable resistivity between nanoscale electronic elements. Ultimately, additional effort is required to achieve full restoration of the graphene lattice. Therefore, TCNL of GF is a promising technique to create GNRs possibly applicable to tunable electronic devices with conductivity modulation.

EXPERIMENTAL SECTION

CVD-grown, single-layer graphene (SLG) on Cu was transferred onto a 100 nm SiO_2/Si substrate using standard PMMA transfer techniques.[26] The SiO_2 surface was precoated with the hydrophobic molecule HMDS to minimize unintentional p-type doping of SLG by moisture adsorbed from the air.[27] The transferred graphene film was then formed into microscale field-effect transistors (FETs) with Ti/Au source and drain electrodes using conventional photolithography. These base FET devices were subsequently annealed at 200 °C under flowing Ar ($t \approx 2-3$ h) and screened to ensure that the Dirac point (or charge neutrality point) was near 0 V gate voltage, indicating a low-doped state. The average sheet resistance of base devices was ~2−3 kΩ/□ with a 4 μm channel length between source and drain. The base graphene devices were then fluorinated by XeF_2 exposure for 900 s (Xactic etcher) to form insulating (>1 TΩ/□) graphene fluoride for TCNL.[11]

Thermochemical nanolithography was performed with the heated AFM probe (UIUC) at varied temperature in contact mode AFM (Multimode AFM, Bruker Co. and Cypher AFM, Asylum Research, CA). The chamber of the AFM was purged with either N_2 or 10% H_2/Ar during TCNL.

Conflict of Interest: The authors declare no competing financial interest.

Acknowledgment. This work was supported by the DARPA Tip-Based Nanofabrication (TBN) program and NRL Nanoscience Institute. M.H. and E.C. acknowledge support from the USNA Trident scholarship program.

Supporting Information Available: (1) Raman spectra of 7 × 7 μm area of reduced graphene fluoride by TCNL. (2) GNRs as narrow as 40 nm wide written by TCNL. This material is available free of charge *via* the Internet at http://pubs.acs.org.

REFERENCES AND NOTES

1. Han, M. Y.; Ozyilmaz, B.; Zhang, Y. B.; Kim, P. Energy Band-Gap Engineering of Graphene Nanoribbons. *Phys. Rev. Lett.* **2007**, *98*, 206805.
2. Li, X. L.; Wang, X. R.; Zhang, L.; Lee, S. W.; Dai, H. J. Chemically Derived, Ultrasmooth Graphene Nanoribbon Semiconductors. *Science* **2008**, *319*, 1229–1232.
3. Kosynkin, D. V.; Higginbotham, A. L.; Sinitskii, A.; Lomeda, J. R.; Dimiev, A.; Price, B. K.; Tour, J. M. Longitudinal Unzipping of Carbon Nanotubes to Form Graphene Nanoribbons. *Nature* **2009**, *458*, 872–877.
4. Bai, J. W.; Duan, X. F.; Huang, Y. Rational Fabrication of Graphene Nanoribbons Using a Nanowire Etch Mask. *Nano Lett.* **2009**, *9*, 2083–2087.
5. Sinitskii, A.; Tour, J. M. Patterning Graphene Nanoribbons Using Copper Oxide Nanowires. *Appl. Phys. Lett.* **2012**, *100*, 103106.
6. Lee, W.-K.; Robinson, J. T.; Gunlycke, D.; Stine, R. R.; Tamanaha, C. R.; King, W. P.; Sheehan, P. E. Chemically Isolated Graphene Nanoribbons Reversibly Formed in Fluorographene Using Polymer Nanowire Masks. *Nano Lett.* **2011**, *11*, 5461–5464.
7. Zhang, K.; Fu, Q.; Pan, N.; Yu, X.; Liu, J.; Luo, Y.; Wang, X.; Yang, J.; Hou, J. Direct Writing of Electronic Devices on Graphene Oxide by Catalytic Scanning Probe Lithography. *Nat. Commun.* **2012**, *3*, 1194.
8. Wei, Z.; Wang, D.; Kim, S.; Kim, S.-Y.; Hu, Y.; Yakes, M. K.; Laracuente, A. R.; Dai, Z.; Marder, S. R.; Berger, C.; *et al.* Tunable Reduction of Graphene Oxide for Graphene Electronics. *Science* **2010**, *328*, 1373–1376.
9. Fletcher, P. C.; Felts, J. R.; Dai, Z. T.; Jacobs, T. D.; Zeng, H. J.; Lee, W.; Sheehan, P. E.; Carlisle, J. A.; Carpick, R. W.; King, W. P. Wear-Resistant Diamond Nanoprobe Tips with Integrated Silicon Heater for Tip-Based Nanomanufacturing. *ACS Nano* **2010**, *4*, 3338–3344.
10. Bagri, A.; Mattevi, C.; Acik, M.; Chabal, Y. J.; Chhowalla, M.; Shenoy, V. B. Structural Evolution during the Reduction of Chemically Derived Graphene Oxide. *Nat. Chem.* **2010**, *2*, 581–587.
11. Robinson, J. T.; Burgess, J. S.; Junkermeier, C. E.; Badescu, S. C.; Reinecke, T. L.; Perkins, F. K.; Zalalutdniov, M. K.; Baldwin, J. W.; Culbertson, J. C.; Sheehan, P. E.; *et al.* Properties of Fluorinated Graphene Films. *Nano Lett.* **2010**, *10*, 3001–3005.
12. Stine, R.; Ciszek, J. W.; Barlow, D. E.; Lee, W. K.; Robinson, J. T.; Sheehan, P. E. High-Density Amine-Terminated Monolayers Formed on Fluorinated CVD-Grown Graphene. *Langmuir* **2012**, *28*, 7957–7961.
13. Elias, D. C.; Nair, R. R.; Mohiuddin, T. M. G.; Morozov, S. V.; Blake, P.; Halsall, M. P.; Ferrari, A. C.; Boukhvalov, D. W.; Katsnelson, M. I.; Geim, A. K.; *et al.* Control of Graphene's Properties by Reversible Hydrogenation: Evidence for Graphane. *Science* **2009**, *323*, 610–613.
14. Baraket, M.; Stine, R.; Lee, W. K.; Robinson, J. T.; Tamanaha, C. R.; Sheehan, P. E.; Walton, S. G. Aminated Graphene for DNA Attachment Produced *via* Plasma Functionalization. *Appl. Phys. Lett.* **2012**, *100*, 233123.

15. Withers, F.; Bointon, T. H.; Dubois, M.; Russo, S.; Craciun, M. F. Nanopatterning of Fluorinated Graphene by Electron Beam Irradiation. *Nano Lett.* **2011**, *11*, 3912–3916.
16. Kwon, S.; Ko, J.-H.; Jeon, K.-J.; Kim, Y.-H.; Park, J. Y. Enhanced Nanoscale Friction on Fluorinated Graphene. *Nano Lett.* **2012**, *12*, 6043–6048.
17. Nair, R. R.; Ren, W.; Jalil, R.; Riaz, I.; Kravets, V. G.; Britnell, L.; Blake, P.; Schedin, F.; Mayorov, A. S.; Yuan, S.; *et al*. Fluorographene: A Two-Dimensional Counterpart of Teflon. *Small* **2010**, *6*, 2877–2884.
18. Cheng, Z. G.; Zhou, Q. Y.; Wang, C. X.; Li, Q. A.; Wang, C.; Fang, Y. Toward Intrinsic Graphene Surfaces: A Systematic Study on Thermal Annealing and Wet-Chemical Treatment of SiO_2-Supported Graphene Devices. *Nano Lett.* **2011**, *11*, 767–771.
19. Lin, Y. C.; Lu, C. C.; Yeh, C. H.; Jin, C. H.; Suenaga, K.; Chiu, P. W. Graphene Annealing: How Clean Can It Be? *Nano Lett.* **2012**, *12*, 414–419.
20. Mattevi, C.; Kim, H.; Chhowalla, M. A Review of Chemical Vapour Deposition of Graphene on Copper. *J. Mater. Chem.* **2011**, *21*, 3324–3334.
21. Pirkle, A.; Chan, J.; Venugopal, A.; Hinojos, D.; Magnuson, C. W.; McDonnell, S.; Colombo, L.; Vogel, E. M.; Ruoff, R. S.; Wallace, R. M. The Effect of Chemical Residues on the Physical and Electrical Properties of Chemical Vapor Deposited Graphene Transferred to SiO_2. *Appl. Phys. Lett.* **2011**, *99*, 122108.
22. Snow, E. S.; Campbell, P. M. AFM Fabrication of Sub-10-Nanometer Metal-Oxide Devices with In-Situ Control of Electrical-Properties. *Science* **1995**, *270*, 1639–1641.
23. Kaiser, A. B.; Skakalova, V. Electronic Conduction in Polymers, Carbon Nanotubes and Graphene. *Chem. Soc. Rev.* **2011**, *40*, 3786–3801.
24. Song, H. S.; Li, S. L.; Miyazaki, H.; Sato, S.; Hayashi, K.; Yamada, A.; Yokoyama, N.; Tsukagoshi, K. Origin of the Relatively Low Transport Mobility of Graphene Grown Through Chemical Vapor Deposition. *Sci. Rep.* **2012**, *2*, 337.
25. Withers, F.; Russo, S.; Dubois, M.; Craciun, M. F. Tuning the Electronic Transport Properties of Graphene through Functionalisation with Fluorine. *Nanoscale Res. Lett.* **2011**, *6*, 526.
26. Li, X. S.; Cai, W. W.; An, J. H.; Kim, S.; Nah, J.; Yang, D. X.; Piner, R.; Velamakanni, A.; Jung, I.; Tutuc, E.; Banerjee, S. K.; Colombo, L.; Ruoff, R. S. Large-Area Synthesis of High-Quality and Uniform Graphene Films on Copper Foils. *Science* **2009**, *324*, 1312–1314.
27. Lafkioti, M.; Krauss, B.; Lohmann, T.; Zschieschang, U.; Klauk, H.; von Klitzing, K.; Smet, J. H. Graphene on a Hydrophobic Substrate: Doping Reduction and Hysteresis Suppression under Ambient Conditions. *Nano Lett.* **2010**, *10*, 1149–1153.